Dalton Transactions

# Hydration of α-$UO_3$ following storage under controlled conditions of temperature and relative humidity

| | |
|---|---|
| Journal: | *Dalton Transactions* |
| Manuscript ID | DT-ART-05-2020-001852.R1 |
| Article Type: | Paper |
| Date Submitted by the Author: | 10-Jul-2020 |
| Complete List of Authors: | Wilkerson, Marianne; Los Alamos National Laboratory, Chemistry Division<br>Hernandez, Sarah; Los Alamos National Laboratory, MST-16<br>Mullen, William; Los Alamos National Laboratory<br>Nelson, Andrew; Oak Ridge National Laboratory, Nuclear Fuel Materials<br>Pugmire, Alison; Los Alamos National Laboratory, Materials Science and Technology<br>Scott, Brian; Los Alamos National Laboratory, Materials Physics and Applications<br>Sooby Wood, Elizabeth; University of Texas at San Antonio<br>Tamasi, Alison; Defense Threat Reduction Agency<br>Wagner, Gregory; Los Alamos National Laboratory<br>Walensky, Justin; University of Missouri, Chemistry |
| | |

ARTICLE

# Hydration of α-$UO_3$ following storage under controlled conditions of temperature and relative humidity

Received 00th January 20xx,
Accepted 00th January 20xx

DOI: 10.1039/x0xx00000x

Marianne P. Wilkerson,*[a] Sarah C. Hernandez,[a] W. Tyler Mullen,[a] Andrew T. Nelson,[a] Alison L. Pugmire,[a] Brian L. Scott,[a] Elizabeth S. Sooby,[a] Alison L. Tamasi,[a,b] Gregory L. Wagner,[a] and Justin R. Walensky[b]

Changes in chemical speciation of uranium oxides following storage under varied conditions of temperature and relative humidity are valuable for characterizing material provenance. In this study, subsamples of high purity α-$UO_3$ were stored under four sets of controlled conditions of temperature and relative humidity over several years, and then measured periodically for chemical speciation. Powder X-ray diffraction (XRD) analysis and extended X-ray absorption fine structure spectroscopy confirm hydration of α-$UO_3$ to a schoepite-like end product following storage under each of the varied storage conditions, but the species formed during exposure to the low relative humidity and lower temperature condition follows different trends from those formed under the other three storage conditions (high relative humidity with high or low temperatures, and low relative humidity with a high temperature). Thermogravimetry coupled with XRD analysis was carried out to distinguish desorption pathways of water from the hydrated end products. Density functional theory calculations discern changes in the structure of α-$UO_3$ following incorporation of 1, 2 or 3 $H_2O$ molecules or 1, 2 or 3 OH groups into the orthorhombic lattice, revealing differences in lattice constants, U-O bond lengths, and U-U distances. The collective results from this analysis are in contrast to analogous studies that report that $U_3O_8$ is oxidized and hydrated in air during storage under high relative humidity conditions.

## Introduction

The chemical reactivity of uranium oxide compounds in oxidizing or hydrating conditions has relevance to many fields, including environmental transport and fate of uranium, storage of uranium oxide fuel, and nuclear processes involving conversion materials.[1-9] In particular, it is proposed that chemical speciation could serve as a useful component of forensic investigations of interdicted materials.[10-15] Such studies submit that correlation of chemical signatures in uranium oxide materials with either industrial processes used for manufacturing or any temporal changes in chemical speciation resulting from storage under controlled temperature (*T*) and relative humidity (RH) could proffer forensic insight into provenance of unknown samples.

Uranium oxide materials, including uranium trioxide ($UO_3$), are formed as chemical intermediates or end-products in processes to separate or purify uranium.[2,16] It is essential to understand the lattice structures of $UO_3$ phases and hydrates, many of which have been published, if one is to measure and model any potential chemical changes in the speciation of these materials. Structural data of $UO_3$ polymorphs and $UO_3$ hydrates are provided in Tables S1 and S2, respectively, in the Supporting Information.[16-50] Studies to determine enthalpies of formation of hydrated $UO_3$ phases and transformations between $UO_3$ hydrates have been conducted.[51-54] The structural analysis of schoepite ($UO_3 \cdot 2.25H_2O$) reveals $[(UO_2)_8O_2(OH)_{12}]$ sheets of pentagonal bipyramidal uranium oxide hydroxide structures.[‡] It is noted that the reflections in the powder X-ray diffraction (XRD) patterns of schoepite and metaschoepite are in close proximity, and typically cannot be discerned from one another if these two species are present as an admixture of the two phases (*vide intra*).[53] These analyses of $UO_3$ hydrates emphasize the amphoteric nature of $H_2O$ to the $[(UO_2)_8O_2(OH)_{12}]$ sheets.

Correlations between calcination reactions to form $UO_3$ polymorphs are reported.[55-58] For example, a recent investigation reviews the chemical phases of $UO_3$ generated by industrially relevant production routes that employ $UO_2(NO_3)_2 \cdot 6H_2O$, $(NH_4)_4UO_2(CO_3)_3$, and $UO_2(O_2) \cdot 2H_2O$ as starting materials.[56] Analyses of the XRD patterns and optical spectra of the products reveal that the $UO_3$ phases that form are associated with the reaction route used to prepare them.

Thermoanalytical methods establish decomposition routes of $UO_3$ materials in order to evaluate bulk physical properties, such as dehydration and decomposition. One study reports measurements of high *T* XRD analysis, scanning electron microscopy, thermal analyses, vibrational (Raman and infrared absorption) spectroscopy, and $^1H$ Nuclear Magnetic Resonance spectroscopy to evaluate thermal decomposition of studtite ($(UO_2)(O_2(H_2O) \cdot 2H_2O)$) to meta-studtite ($(UO_2)O_2(H_2O)_2$) and α-

[a] Los Alamos National Laboratory, Los Alamos, New Mexico 87545, United States
[b] Department of Chemistry, University of Missouri-Columbia, Columbia, Missouri 65211, United States

Electronic Supplementary Information (ESI) available: [details of any supplementary information available should be included here]. See DOI: 10.1039/x0xx00000x

$UO_3$.[55] The analysis suggests formation of an amorphous $UO_3$ intermediate, formulated as sub-stoichiometric $UO_{3-x}(OH)_{2x}{\cdot}zH_2O$, prior to decomposition to $\alpha$-$UO_3$ and then $\alpha$-$U_3O_8$ after continued heating.

Other work suggests that compounds with lower oxidation states of uranium, such as $U_3O_8$ and $UO_2$, may be oxidized and hydrated following exposure to environmental conditions.[11,52,53] A report to model the formation of secondary phases following release of anthropogenic uranium into the natural environmental indicates that schoepites are present in acidic to neutral pH conditions.[52] Oxidation of uranium dioxide ($UO_2$) occurs following temporal exposure to a moist environment.[5,6]

Although the uranium in $UO_3$ is already in its highest oxidation state, U(VI) anhydrous phases are prone to hydration, and a study to evaluate any changes in chemical speciation of $UO_3$ itself would be useful for forensic analyses. The objective of the current study is to characterize hydration of phase pure $\alpha$-$UO_3$ following storage under controlled *T* and RH for up to five years. Subsamples were measured periodically, and results are assessed for changes in chemical speciation. Powder-XRD patterns and extended X-ray absorption fine structure (EXAFS) measure changes in the long-range and short-range structural order, respectively. Thermogravimetric analysis (TGA) coupled with XRD analysis provide evaluation of the phases formed during dehydration of subsamples that had been stored under controlled conditions of *T* and RH for 5 years. Theoretical studies using density functional theory (DFT) offer insight into the complex interplay between covalent and ionic U-O interactions, and the structural disorder between interstitial $H_2O$ molecules and OH groups. This approach affords a means for understanding bulk chemical properties of these hydrated materials and perturbations to the lattice structure, and provides a model of the intermolecular interactions involved in the hydration of $\alpha$-$UO_3$.

## Experimental

**Materials and syntheses**

The preparation of $\alpha$-$UO_3$ is described elsewhere.[10] The phase purity of the hexagonal structure of the beige $\alpha$-$UO_3$ was confirmed by XRD analysis, as shown in Figure 1a.[24]

**Storage under controlled temperature and relative humidity**

Aging vessels fabricated from Swagelok fittings are described elsewhere.[11,59-61] The four storage conditions of *T* and RH included Condition 1 (5 °C, 25% RH), Condition 2 (37 °C, 15% RH), Condition 3 (5 °C, 97% RH), and Condition 4 (37 °C, 89% RH), and are given in Table S3, Supporting Information along with respective water vapour densities. Saturated lithium iodide aqueous solutions were used to achieve the lower RH conditions, and saturated potassium nitrate aqueous solutions were used to establish the higher RH conditions. Time 0 for $\alpha$-$UO_3$ is defined as the time at which the synthesis of the material was completed. Average conditions in our laboratory were 20 °C and ~20% RH.

**Powder X-ray diffraction (XRD) analysis**

Powder-XRD patterns of freshly prepared $\alpha$-$UO_3$ at time 0 were collected on a Bruker D8 Discover diffractometer equipped with either a Hi-Star area detector or a high resolution NiI scintillation detector and monochromatized Cu K$\alpha$ X-rays. Powder-XRD patterns of $UO_3$ material stored for 2-3.5 years under Conditions 1–4 were collected on a Bruker D8 Advance diffractometer equipped with a Lynxeye 1-D silicon strip detector and unconditioned Cu K$\alpha$ X-rays. Qualitative analyses were performed using JADE 9.0 software and the 2014 PDF-4+ database. Slight nonstoichiometries in hydration or oxygen content could produce variations between reference lines reported for a given chemical species. In some cases, reflections were challenging to assign to distinct schoepite phases because patterns from inter-grown schoepite and meta-schoepite are likely not resolvable.[52,53] As described below under **Thermogravimetric (TGA) analysis**, the chemical speciation of the intermediate species formed at TGA temperature plateaus were measured by XRD analysis with a Bruker D2 Phaser diffractometer.

**Extended X-ray absorption fine structure (EXAFS) spectroscopy, sample preparation, and data collection**

Samples and subsamples were prepared for EXAFS measurements as described in reference 11. All data were collected at 77 K on beamline 11-2 at the Stanford Synchrotron Radiation Lightsource (SSRL) at SLAC National Accelerator Laboratory. Data were acquired up to $k$ ~ 15.2 Å$^{-1}$, and the $k^3$-weighted U $L_{III}$-edge data were transformed between $k$ = [2.5 – 15.0 Å$^{-1}$] and narrowed by a Gaussian window of 0.3 Å$^{-1}$. The data were fit using U-O and U-U shells between $R$ = [1.5 Å – 6.5 Å]. Two identical scattering shells (e.g. U-O) were only included if they met the following shell resolution criterion, $\Delta R \geq \pi/2\,\Delta k$.[62] The EXAFS oscillations were extracted from the total EXAFS absorption spectrum.[63,64] Data reduction and analyses were performed using RSXAP analysis codes.[64,65] Theoretical amplitudes and phase functions were generated from relevant crystal structures using the FEFF7 code.[66]

**Thermogravimetric (TGA) analysis**

The thermal stability and dehydration profiles of $UO_3$ material stored for five years under Conditions 1-4 were investigated using TGA on a Netzsch 449 F3 simultaneous thermal analyser (STA) equipped with alumina fixturing.[67] Powders weighing 40-50 mg were heated under flowing $O_2$ (200 mL/min) and Ar (20mL/min) from room *T* to 1000 °C with a heating rate of 10 °C/min, and the instantaneous weight of the material was recorded within 0.001 mg as a function of *T*. Two TGA runs were performed for each condition, and the corresponding decomposition profiles are consistent. The data for only one condition is reported for each condition in Figure 3 for simplicity. Oxygen was used instead of pure argon to ensure that the heated $UO_3{\cdot}xH_2O$ would be thermodynamically stable as dictated by the system oxygen activity. Calibration of the thermocouple was performed using the melting points of pure indium, tin, bismuth, zinc, and aluminium, thereby spanning the *T* range relevant to the present work. Results of these melting point calibrations were used to state the accuracy of *T* reported to ± 2K. Data were baseline corrected to account for the buoyancy effect by measuring a heated empty crucible under

the prescribed temperature profile. All reaction onsets reported in this study were determined using Netzsch Proteus software, Version 6.1. Temperature plateaus in which the mass did not change over a *T* range were measured, and the chemical speciation of the intermediate species formed at these temperature plateaus were measured by XRD analysis with a Bruker D2 Phaser diffractometer as described above under **Powder X-ray diffraction (XRD) analysis**.

**Computational methodology**

Density functional theory calculations to model hydration of α-$UO_3$ were implemented in VASP,[68-72] and employed the generalized gradient approximation (Perdew-Burke-Ernzerhof)[73] to the exchange-correlation functional with Hubbard *U* correction (GGA+U).[74]

The lattice parameters and space groups for modelling perturbations of the α-$UO_3$ lattice following incorporation of $H_2O$ molecules or OH groups were selected based upon an evaluation of reported structures, provided in Table S1, Supporting Information. A discussion of this evaluation is included under Table S1, Supporting Information.[16-34] The orthorhombic *C2mm* structure proposed by Cordfunke and Loopstra was applied to these simulations.[20] A 3 x 2 x 3 supercell was employed to model the α-$UO_3$ structure, which yields 18 $UO_3$ unit cells or 36 $UO_3$ molecules. As reported by Brincat et al., a *U* value of 4.5 eV and *J* value of 0.54 eV was applied only to the U 5*f* electronic states.[16] Parameters include a kinetic plane-wave energy of 500 eV and energy convergence of 1 x $10^{-5}$ eV. The volume (including lattice constants and angles) and atomic positions of the ions were relaxed until the Hellmann-Feynman forces on each ion were less than 1 x $10^{-2}$ eV/Å. A Γ-centered Monkhorst-Pack 2 x 2 x 2 k-point mesh was useful for all calculations, since total energies converged within less than 1 MeV when compared to denser k-point meshes. Magnetic configuration or spin-orbit coupling was not considered since the U 5*f*$^0$ configuration implies that there is no magnetic moment on the U atoms. Therefore, all calculations were performed at the no-spin-polarization level of theory.

To model hydrated α-$UO_3$, 1, 2 or 3 interstitial $H_2O$ molecules, or 1, 2 or 3 OH groups were added to the center of the α-$UO_3$ supercell, and the structures were allowed to fully relax to their lowest energy state. Visualization and simulated XRD patterns were carried out using the VESTA program.[75,76]

## Results and discussion

### Structural characterization of α-$UO_3$ and hydration products

Initially, freshly prepared amorphous $UO_3$ was stored under high relative humidity conditions (Conditions 3 and 4) but a damp and intractable material formed, precluding delicate sample handling and accurate measurement of chemical structures. Synthesis of high purity α-$UO_3$ by calcination of $UO_2(O_2)\cdot x H_2O$ was selected because the product was characterized by an ordered lattice and was readily manipulated.[10] This reaction route does not include carbon-, fluoride-, or nitrogen-containing intermediates typically used in industrial-scale processes.[2] As shown in Figure 1a, XRD analysis revealed that the beige material is pure hexagonal α-$UO_3$ (hexagonal) with no measurable peaks from potential impurities.[19-22,24]

The α-$UO_3$ powder was divided into four subsamples that were stored under each condition of controlled *T* and RH described in Experimental and listed in Table S3, Supporting Information. Powder-XRD patterns were collected from subsamples after storage for 14 months and for 2.5 years.[11,59-61] These XRD patterns are compared with the pattern of freshly prepared α-$UO_3$ in Figure 1. The reflections contributed by $UO_3\cdot x H_2O$ are marked with an asterisk. In particular, a reflection at ~12° in 2θ characteristic of $UO_3\cdot x H_2O$ is present in the XRD patterns of the subsamples stored under Conditions 2, 3 and 4 for 14 months and for 2.5 years, as well as Condition 1 after 2.5 years. This reflection is notably absent in the pattern of the subsample stored under Condition 1 for 14 months. These results suggest that hydration of α-$UO_3$ eventually occurs even under mild conditions of *T* and RH. The reflection at ~21° in 2θ characteristic of α-$UO_3$ is prominent in the spectrum of α-$UO_3$ stored for 14 months under Condition 1 and is weakly apparent in the patterns of the subsample stored under Condition 2 for 14 months. It is not present in the other 6 XRD patterns. This outcome differs from the oxidation and hydration of subsamples of α-$U_3O_8$ for which the XRD patterns for samples stored under low RH (Conditions 1 and 2) did not show evidence for $UO_3\cdot x H_2O$, suggestive that elevated RH was essential for chemical oxidation and hydration of α-$U_3O_8$.[11]

We collected U $L_{III}$ EXAFS measurements in order to probe local order and subtle changes in bonding and coordination around the uranium atoms. EXAFS data were acquired from α-$UO_3$ at time 0 and following storage under Conditions 1-4 for 0.5 and 3 years. The spectrum of freshly prepared α-$UO_3$ is provided in Figure 2(a). Two regions of scatterers were measured: uranium-oxygen (U-O) paths between $R$ - $\theta$ ~ 1.9 Å – 2.5 Å and uranium-uranium (U-U) paths between $R$ - $\theta$ ~ 3.7 Å – 4.2 Å. The two peaks were modelled with scattering paths generated from the crystal structure of orthorhombic α-$UO_3$ (ICSD = 15567) using FEFF7 (orthorhombic, Tables S4 and S5, Supporting Information; Figures S1-S9, Supporting Information)[65,77] and these regions correspond to U-O bond distances at $R$ ~ 1.8 – 2.4 Å and U-U distances at $R$ ~ 3.7 – 4.1 Å. The refined distances were consistent with those reported by Loopstra and Cordfunke,[20] while attempts to include additional paths proposed in the structural analysis by Greaves and Fender did not statistically improve the fit.[17]

Comparison of the EXAFS measurements of freshly prepared α-$UO_3$ (Figure 2(a)) with spectra collected from the subsamples stored for 6 months and 3 years under Conditions 1-4 (Figures 2(b-i)) suggests that all four conditions affect the chemical speciation even after storage for 6 months. In the EXAFS spectra of α-$UO_3$ stored under Conditions 2, 3 and 4, the U-O paths in the region of $R$ ~ 1.9 – 2.0 Å were fitted with multiple shells of U-O scatterers characteristics of a hydrated, schoepite-like species.[39] The amplitudes of the U-O shell are more intense in subsamples stored under Conditions 2, 3 and 4 than that of the α-$UO_3$ at time 0. Unlike previously reported EXAFS spectra of schoepite, no amplitude was observed in the U-U region ($R$ ~ 3.8

Å) of these spectra of subsamples stored under Conditions 2, 3 or 4, consistent with disorder of the uranium atoms following storage.

The EXAFS spectra of the subsample stored under Condition 1 for 6 months and 3 years, however, reveal a different trend from the spectra measured from subsamples stored under Conditions 2, 3 and 4, and suggest that a different species formed within 6 months and persisted for at least 3 years. The distances of the U-O paths were between those of freshly prepared $\alpha$-$UO_3$ (Figure 1(a)) and the schoepite-like subsamples stored under Conditions 2, 3 and 4 (Figure 1(d-i)), and the amplitudes of both the U-O and U-U paths were relatively weaker than those recorded for $\alpha$-$UO_3$, likely due to disorder in the lattice structure.

A photograph to compare freshly-prepared $\alpha$-$UO_3$ and subsamples stored for 5 years under Conditions 1, 3 and 4 is provided in Graphic 1. The subsample stored under Condition 1 for 5 years was beige, suggestive that it was similar to the original material (Graphic 1(1) and Graphic 1(4)). In contrast, subsamples stored under high RH conditions (Condition 3 (Graphic 1(3) and Condition 4 (Graphic 1(2)) were bright yellow, the color of schoepites.[2] This visual observation is consistent with analyses that suggest that $\alpha$-$UO_3$ is not fully hydrated under cool and dry conditions. (Note that there was no remaining subsample stored under Condition 2 for comparison with the other 3 stored subsamples after 5 years.)

The XRD pattern (Figure S10, Supporting Information) collected on the D2 Phaser, and the beige color noted for the subsample stored under Condition 1 for 5 years suggests that the material could be a mixture of $UO_3{\cdot}xH_2O$ and $\alpha$-$UO_3$.

It is notable that the EXAFS spectra collected from subsamples stored under each Condition for 6 months versus 3 years are identical. These similarities suggest that an equilibrium $UO_3{\cdot}xH_2O$ species was achieved by 6 months following storage under any of the four Conditions, such that once a chemical intermediate formed, changes in hydration and/or chemical speciation did not proceed within this timeframe. This result was in contrast to the chemical speciation of $\alpha$-$U_3O_8$ formed after storage under these four Conditions in which changes in chemical speciation occurred gradually and continuously until a schoepite endpoint was reached. Comparison of these EXAFS spectra with the XRD patterns suggests temporal changes in the long-range lattice structure to schoepite following storage under all conditions, but with different perturbations of the U-O and U-U local order for subsamples stored under Condition 1 compared to subsamples stored under Conditions 2, 3 and 4. The spectrum of the subsample stored under Condition 1 suggests chemical speciation that developed from a different reaction pathway.

A separate study was carried out to evaluate if the hydration of $\alpha$-$UO_3$ initialized rapidly. An *in situ* experiment to measure XRD patterns of $\alpha$-$UO_3$ held under 60 °C and 70% RH, conditions available to this instrument, was carried out on the goniometer for 5 days. No change in the XRD patterns from the original $\alpha$-$UO_3$ were measured, suggestive that any changes in the ordered phase structure likely occur on the timescale of months.

**Dehydration of $UO_3{\cdot}xH_2O$**

Any differences between the decomposition of the $\alpha$-$UO_3$ and the subsamples stored under Conditions 1-4 could be indicative of differences between chemical reactivity during hydration. A baseline TGA measurement of $\alpha$-$UO_3$ heated under pure $O_2$, shown in Figure 3a, was heated to the highest *T* possible for this setup. The profile reveals minimal mass change until a defined step is observed between 650-652 °C, indicating a mass loss of 1.87%. An XRD pattern of the product formed at this *T* is in agreement with that of $\alpha$-$U_3O_8$ (PDF-00-047-1493) with no unidentified reflections. Thermochemical models developed for the uranium oxygen binary system report that this solid-solid transformation between $\alpha$-$UO_3$ and $\alpha$-$U_3O_8$ occurs at 650-670 °C.

Subsequently, TGA measurements from $\alpha$-$UO_3$ stored for 5 years under Conditions 1, 3 and 4 for 5 years were carried out, and these decomposition traces are given in Figure 3b-d, respectively. The decomposition trace measured from the subsample stored under Condition 1 for 5 years is shown in Figure 3b. The trace exhibits gradual mass loss from room *T* to 642 °C, likely due to loss of adsorbed $H_2O$ followed by decomposition to $\alpha$-$U_3O_8$ at ~642 °C, consistent with the decomposition curve of $\alpha$-$UO_3$.[20-22] This similarity suggests that the chemical speciation of this subsample is characteristic of a $UO_3$ stoichiometry.

The subsamples stored under Conditions 3 and 4 go through different intermediate chemical compositions than the subsample stored under Condition 1. The decomposition traces measured from the hydrate $\alpha$-$UO_3$ subsamples stored under higher RH (Conditions 3 and 4) for 5 years are shown in Figure 3c and 3d. The decomposition curves reveal different behaviour in that sharp mass losses are apparent in the temperature range 150-250 °C, likely due to desorption of one $H_2O$ molecule. These two subsamples continue to lose mass with increased *T* until formation of poorly crystalline orange $U_3O_8$ at ~380 °C (Figure 3, Plateau 1). Following continued heating, the materials undergo a smaller mass loss until the formation of brown anhydrous $UO_3$ material at 515-520 °C (Figure 3, Plateau 2). Final mass loss occurred from decomposition of $UO_3$ to $U_3O_8$ at 635-640 °C. The observation that the decomposition curves of these two subsamples overlap implies that both materials are similar, but of a different composition than those of the freshly prepared $\alpha$-$UO_3$ and the subsample stored under Condition 1. These analyses are consistent with the EXAFS results (*vide supra*).

As noted above in the discussion of the TGA measurements from freshly prepared $\alpha$-$UO_3$ and material stored under Condition 1, the final weight loss measured from the subsamples stored under Conditions 3 and 4 was greater than would be predicted if the final product were stoichiometric $U_3O_8$. While it is likely that the subsamples stored for 5 years under Conditions 3 and 4 were slightly less hydrated than stoichiometric $UO_3{\cdot}2.25H_2O$ or $UO_3{\cdot}2H_2O$, the mass losses were ~1.8% lower than predicted following thermal reduction of all materials. One explanation is that the $\alpha$-$UO_3$ starting material was not stoichiometric, but contained $UO_{2.9}$.[18-21,55] Previous

work to characterize the decomposition of uranyl peroxide ($UO_2(O_2)$)·$xH_2O$, $x$ = 2,4) reported the presence of $UO_{2.9}$ in material that is isostructural with $\alpha$-$UO_3$. If the molecular weight of $\alpha$-$UO_3$ prepared for this report is indeed oxygen deficient $UO_{2.9}$, then the predicted mass loss to $U_3O_8$ is not 1.8%, but rather 1.3%, which is in better agreement with the mass loss from $\alpha$-$UO_3$ and the subsample stored under Condition 1.

**Modelling hydration of $\alpha$-$UO_3$**

*Ab initio* computational methods were employed to provide insight into the intermolecular reactivity between $\alpha$-$UO_3$ and interstitial species leading to lattice perturbations of $\alpha$-$UO_3$ and formation of schoepite structures. Former work has shown that not only is $H_2O$ essential to these hydration processes, but also OH groups are important components in many hydrated structures. Density functional theory calculations were carried out to determine the changes in lattice parameters of $\alpha$-$UO_3$ following the addition of between one and three $H_2O$ interstitial molecules or between one and 3 OH interstitial groups (to mimic dissociation of $H_2O$ within the lattice). All fully relaxed lattice constants are provided in Table S6, Supporting Information. The relaxed $\alpha$-$UO_3$ structure is illustrated in Figure 4, and many hydrated structures and simulated XRD patterns are shown in Figure 5 ($UO_3$ and interstitial $H_2O$) and Figure 6 ($UO_3$ and interstitial OH groups).

Relaxation of the atomic positions and the unit cell volume of orthorhombic $\alpha$-$UO_3$ yielded theoretical lattice constants $a$ = 3.95 Å, $b$ = 6.83 Å, and $c$ = 4.18 Å, with percent differences of 0.20%, 0.49%, and 0.25%, respectively. (See Table S6, Supporting Information). The theoretical U-O and U-U distances (U-O1, 2.088 Å; U-O2, 2.279 Å; U-U, 3.847 Å) of relaxed $\alpha$-$UO_3$ are within range of the distances of the U-O and U-U shells revealed in the EXAFS spectra of $\alpha$-$UO_3$ shown in Figure 2, and are in agreement with the experimental distances determined by XRD analysis (Figure 1). Lattice parameters calculated after relaxation of the $\alpha$-$UO_3$ with $H_2O$ molecules or OH group interstitials are given in Table S6, Supporting Information, and the lengths of the U-O1, U-O2, and U-U distances are given in Tables S7, Supporting Information, and the bond lengths and angles of the $H_2O$ molecules and OH groups are given in Table S8, Supporting Information.

Comparable changes were observed in the structure of $\alpha$-$UO_3$ following addition of either one $H_2O$ or one OH group to the lattice (Figures 5b and 6b). The $b$ lattice parameter contracted in both cases, (%$\Delta b$ = -6.70 after addition of $H_2O$; %$\Delta b$ = -4.97 after addition of OH), while lattice parameters $a$ and $c$ expanded by %$\Delta a$ = 8.32 and %$\Delta c$ = 2.08, respectively, after addition of $H_2O$, and by %$\Delta a$ = 9.98 and %$\Delta c$ = 3.07, respectively, after addition of OH. In both cases, modification of lattice resulted in contraction of the U-O1 bond distances to shorter uranyl U-oxo distances of 1.895 Å after addition of one $H_2O$ molecule and 1.876 Å following addition of one OH group, inducing breakdown of the –oxo-U-oxo-U-oxo- chains, as indicated by a loss of 56.9% and 59.7%, respectively, of the initial theoretical U-O1 bonds.

The theoretical equatorial (110) U-O2 bond distances also decreased, and the hexagonal bipyramidal coordination environments around the U atoms relaxed significantly, leading to only 20.4% and 38.0%, respectively, of the initial U-O2 bonds existing in the structure. The contraction of the theoretical bond lengths and distortions of the lattice yields a significant loss of the initial U-U distances (67.4% for $H_2O$ and 71.2% for OH). This model is consistent with the trend of the amplitudes of the U-U shell measured from the EXAFS spectra of the $\alpha$-$UO_3$ subsample stored under Condition 1 (Figure 2b). As shown in Table S8, Supporting Information, the O-H bond stretched for the interstitial $H_2O$, making the H-O-H bond angle larger, and the O-H bond distance of the interstitial OH group also increased.

Chemical reactivity between $\alpha$-$UO_3$ and water was apparent as the number of interstitial $H_2O$ in the model increased to two or three, such that there was structural expansion of the uranium oxide lattice (as shown in Table S6, Supporting Information), and dissociation and recombination of the $H_2O$ molecules is calculated. After addition of two $H_2O$ molecules and relaxation of the lattice, the theoretical $a$, $b$, and $c$ lattice constants increased to 4.29 Å, 7.18 Å, and 4.32 Å, respectively, and relaxation of the O2 atoms from the distorted hexagonal bipyramidal structure was greater than relaxation of O2 following addition of only one water molecule. Approximately 83.2% of the U-U bonds within the modelled structure contracted to ~3.76 Å. Similar results were calculated following theoretical addition of three interstitial $H_2O$ molecules such that incorporation of three $H_2O$ molecules yielded lattice constants 4.02 Å, 7.46 Å, and 4.33 Å. The average U-O1 bond lengths calculated are consistent with the uranyl U-oxo bond length measured in the U-O shell recorded in the EXAFS spectra of $\alpha$-$UO_3$ subsamples stored under Conditions 1-4 for three years. (See Table S5, Supporting Information) There was a similar decrease in the theoretical U-U distances, but the U-O2 bond distance decreased to 1.876 Å and only 13.4% of the theoretical $\alpha$-$UO_3$ bonds were retained. The simulated XRD pattern (Figure 5c, d) reveals low angle peaks at $2\theta < 20°$. These peaks are not apparent in the simulated XRD of $\alpha$-$UO_3$ lattice hosting one interstitial $H_2O$ molecule or OH group. (See Figure 5b and Figure 6b). While the calculated XRD patterns do not perfectly match the measured hydrated UO phases, they do produce additional peaks upon hydration that match the complexity in the general $2\theta$ regions of the measured samples. Due to the complexity of these materials, including disorder in the ionic $OH^-/H_2O$ sub-lattice, perfect agreement is essentially not possible. However, the modelling does capture important structural changes such as the evolution of U-U distances as measured in the EXAFS spectra.

The decrease in the U-O2 bond lengths and U-U distances and expansion of the $\alpha$-$UO_3$ lattice simulated by the DFT calculations is attributed to dissociation and recombination of the interstitial $H_2O$ molecules. (See Table S8, Supporting Information) When two interstitial $H_2O$ molecules are introduced into the lattice, $H_2O$ dissociates to four OH groups and one $O_2$ molecule coordinated with U atoms thus forming a bidentate bonding of a presumed $O_2^{2-}$ peroxide ligand to lattice U atoms (e.g. studtite) with average U-O distance of ~2.499 Å.

The formation of these new species in the structure were formed with O2 atoms. The O-H calculated bond distances of the coordinated OH groups are typical of hydroxide ligands (0.970 Å). The model suggests that the peroxide ligand bridge bonds between the oxygen atom from an $H_2O$ molecule and an equatorial (110) O2 atom, and has an O-O bond length typical of the $O_2^{2-}$ ligand. (See Figure 5c) Addition of three $H_2O$ molecules to the $\alpha$-$UO_3$ lattice into the model reveals dissociation and recombination of the water, forming $H_2O$, OH, and $O_2$ species associating bonding to the O2 lattice atoms. (See Figure 5d) Contrary to when there are two $H_2O$ molecules, the interstitial O and O2 atoms combine to form a monodentate bonding of a bridging $O_2^{2-}$ peroxide ligand coordinated to lattice U atoms with calculated average U-O distances of ~2.207 Å.

In comparison, the presence of two OH groups in the $\alpha$-$UO_3$ lattice model resulted in the contraction of the *b* lattice constant to 6.49 Å and expansion of the *a* and *c* lattice constants to 4.32 Å and 4.52 Å, respectively. Three lattice constants, *a*, *b* and *c*, increased following incorporation of three OH groups. The calculated decrease in the U-O2 bond lengths and the U-U distance likely occurs following dissociation and recombination of the OH groups with lattice O2 atoms forming other OH, and only the bidentate bonding of an $O_2^{2-}$ peroxide ligand with U atoms formed having an average U-O bond length of ~2.63 Å. The formation of a monodentate versus bidentate bonding of a presumed peroxide ligand is evaluated by the existence of $H_2O$ still present in the structure. Based on these DFT calculations, if dissociation of $H_2O$ does not occur within the $\alpha$-$UO_3$ structure, then there is likely a different bonding mechanism for the peroxide (monodentate); otherwise complete dissociation of $H_2O$ will only form the bidentate peroxide.

In all cases, the modelled U-U distances converged to ~3.8 Å and only ~16.6% of the initial distances were retained. The number of U-O1 bonds were preserved steadily in ~41.0% of the initial bonds, while the number of U-O2 bonds decreased along with increased reactivity with lattice O2 atoms, a result of the O2 participating in forming additional species within the structure. These theoretical results are consistent with the absence of absorption intensity in the U-U shell of the EXAFS spectra collected from $\alpha$-$UO_3$ subsamples stored under Conditions 2, 3 and 4 for 0.5 and 3 years. These models are not consistent with the XRD patterns of the subsamples stored under Conditions 1-4 as the simulated XRD patterns reveal relatively weaker reflections.

In order to assess any changes in the electronic structures resulting from increases in the lattice volumes and decreases in the distances between lattice atoms, charge density difference plots were generated from the unperturbed, relaxed $\alpha$-$UO_3$ structure, and the relaxed structure of $\alpha$-$UO_3$ following the addition of three $H_2O$ molecules or three OH groups into the lattice. (See Figures 7 and 8, respectively) Charge accumulation is modeled in the $\alpha$-$UO_3$ lattice between the U-O1 bonds (shown in red), which is suggestive of covalent bonding. In contrast, charge depletion was noted in the equatorial U-O2 bonds (shown in blue) around the U atoms and charge accumulation is observed around the O2 atoms, implying ionic bonding. Following the addition of three $H_2O$ molecules to the lattice, the model suggests covalent bonding in the U-O1 and U-O2 bonds (see Figure 8a), but following addition of three OH groups to the lattice, covalent bonding between U-O1 and U-O2 is modelled, along with bridging of U atoms by O2 atoms. (See Figure 8b) This propensity for covalent bonding following hydration by a greater number of $H_2O$ molecules may explain the diminishing amplitude of the U-U shell in the EXAFS spectra, the shortening of the U-O1 and U-O2 bonds, and the changes in lattice structure. The ionic bonding of U-O2 versus the covalent bond of U-O1 suggest the propensity to form $H_2O$, OH groups and peroxide following hydration of $\alpha$-$UO_3$, and dissociation of $H_2O$ will determine the bonding characteristics of the peroxide.

## Conclusions

This work was conducted to increase the understanding of the chemical speciation of hydrated $\alpha$-$UO_3$. High purity $\alpha$-$UO_3$ was stored under conditions of controlled *T* and RH for up to 5 years, and then characterized by XRD analysis and EXAFS measurements. Following storage under Conditions 1 and 2, XRD data revealed that an intermediate phase formed within 6 months, and then converted to schoepites over time, while crystalline $\alpha$-$UO_3$ material converted to schoepites following storage under Conditions 3 and 4 after 6 months. An intermediate phase with short-range order is observed in EXAFS spectra of subsamples stored under conditions of low relative humidity and low *T* (Condition 1). Thermogravimetric analyses afford the ability to monitor the thermal decomposition of the $UO_3{\cdot}xH_2O$ that formed as a function of storage condition, and reveals formation of two different types of amorphous $UO_3{\cdot}xH_2O$. Density functional theory calculations reveal that hydration of $\alpha$-$UO_3$ induces short U-O bonds and the decrease in U-U distances due to the increased covalent bonding formed between U and lattice oxygen atoms. Dissociation of $H_2O$ will determine the chemical bonding mechanisms of the induced peroxide within the $\alpha$-$UO_3$ structure. These results underscore the complexity involved in hydration of uranium oxide systems.

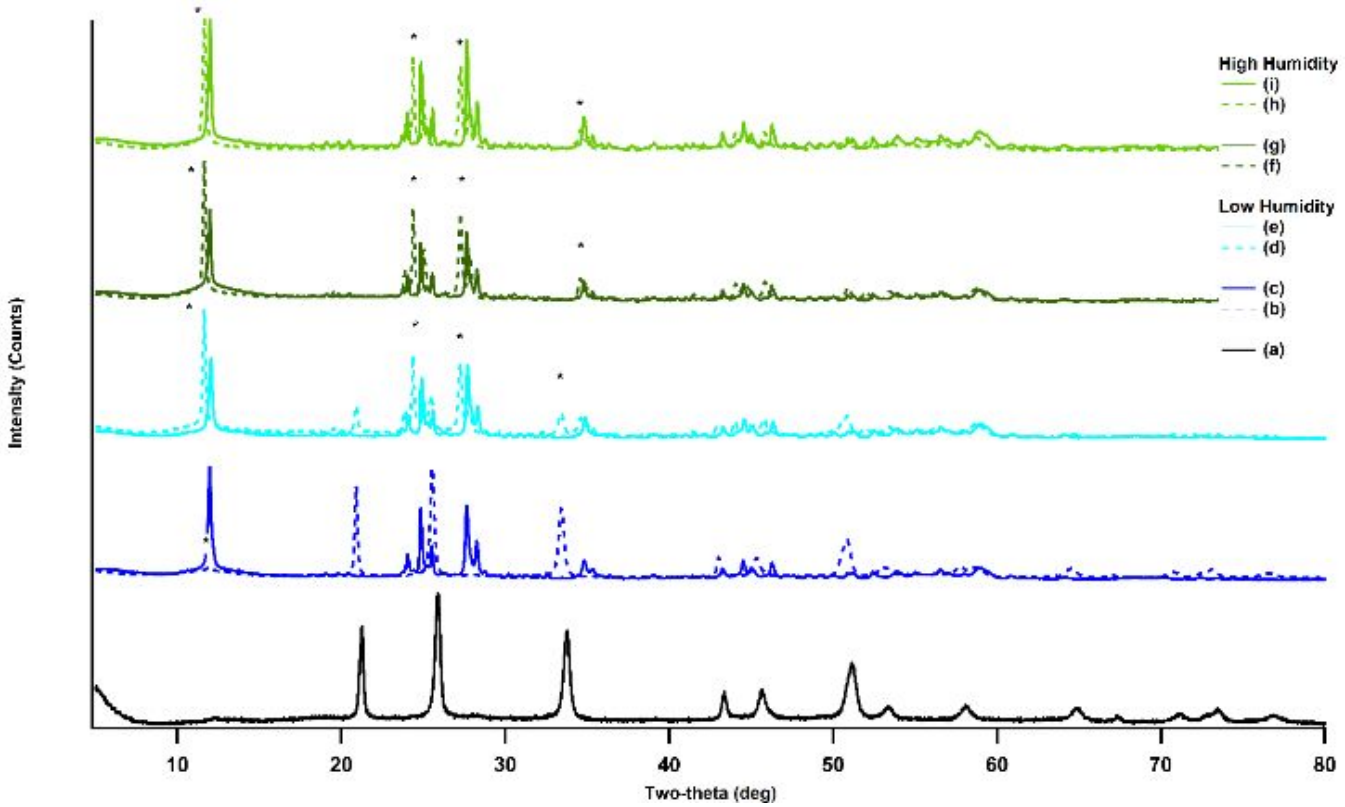


Figure 1. X-ray diffraction analysis patterns of $\alpha$-$UO_3$ (PDF 00-012-0043) at time 0 (solid black line) and after storage for 14 months (dashed coloured lines) and 2.5 years (solid coloured lines) under low RH (blue) and high RH (green). (a) $\alpha$-$UO_3$ (hexagonal phase) at time 0.[24] (b) Condition 1 after 14 months. (c) Condition 1 after 2.5 years. (d) Condition 2 after 14 months. (e) Condition 2 after 2.5 years. (f) Condition 3 after 14 months. (g) Condition 3 after 2.5 years. (h) Condition 4 after 14 months. (i) Condition 4 after 2.5 years. The marked phases (*) correspond to $UO_3 \cdot xH_2O$ (schoepite, PDF 00-050-1601) and $UO_3 \cdot 2H_2O$ (meta-schoepite, PDF 01-075-8796).

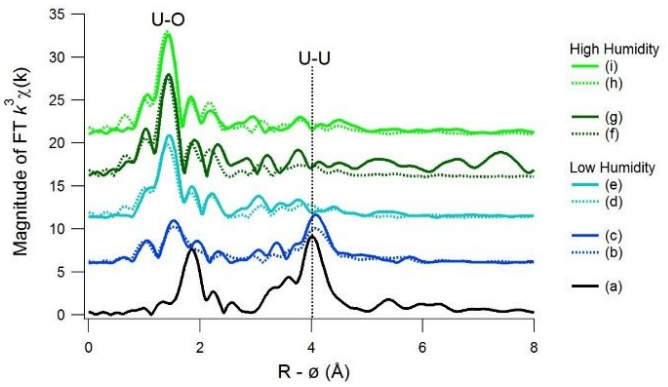


Figure 2. Fourier Transforms (FTs) of U $L_{III}$ EXAFS data for α-$UO_3$ at time 0 (solid black line) and after storage for 0.5 (dashed coloured line) and 3 (solid coloured lines) years under low RH (blue) and high RH (green). (a) α-$UO_3$ at time 0. (b) Condition 1 after 0.5 years. (c) Condition 1 after 3 years. (d) Condition 2 after 0.5 years. (e) Condition 2 after 3 years. (f) Condition 3 after 0.5 years. (g) Condition 3 after 3 years. (h) Condition 4 after 0.5 years. (i) Condition 4 after 3 years.

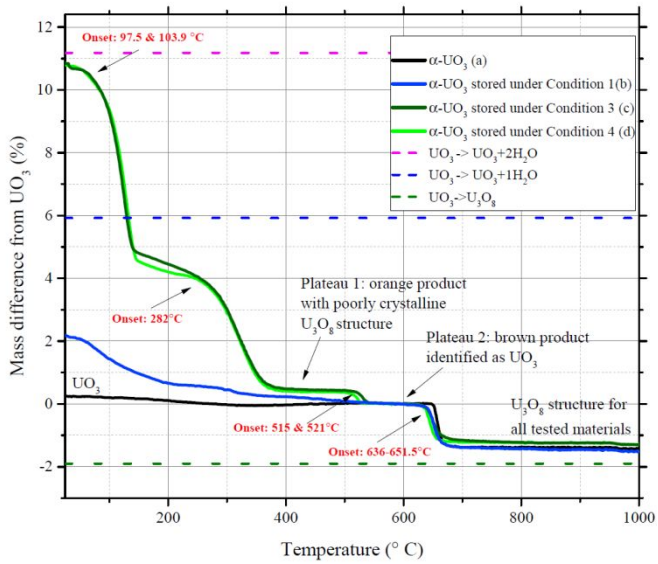


Figure 3. Thermogravimetric analysis showing traces of the % mass difference between freshly prepared α-$UO_3$ versus α-$UO_3$ subsamples stored for 5 years under Condition 1, 3 and 4 as a function of *T* (°C). Heating was conducted under pure $O_2$. Zero mass difference on the y-axis represents the mass of $UO_3$. Plateaus representing theoretical mass differences between uranium oxides $UO_3 \cdot 2H_2O$ and $UO_3$ (red dash), $UO_3 \cdot H_2O$ and $UO_3$ (blue dash), and $UO_3$ and $U_3O_8$ (green dash) are represented by dashed lines. Experimentally measured mass changes of α-$UO_3$ (a, black line), α-$UO_3$ stored under Condition 1 (b, blue line), α-$UO_3$ stored under Condition 4 (c, dark green line), and α-$UO_3$ stored under Condition 3 (light green line) are represented by solid lines. X-ray diffraction analyses reveal that the chemical species formed at Plateau 1 had a poorly crystalline $U_3O_8$ structure, the chemical species formed at Plateau 2 was a brown $UO_3$ product, and the chemical species formed at the final Plateau was α-$U_3O_8$.

Note: The % mass difference between the profile of α-$UO_3$ and the profiles of the other samples were shifted such that the decomposition traces cross the zero point of the y-axis at the same *T* at which the α-$UO_3$ decomposed to α-$U_3O_8$.

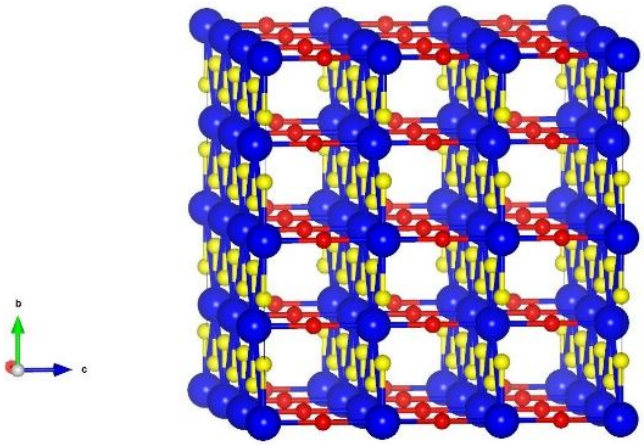


Figure 4. Structure of theoretically relaxed α-$UO_3$. The U atoms (blue) and O1 site atoms (red) form the uranyl-type group, while O2 sites (yellow) lie in the equatorial (110) plane.

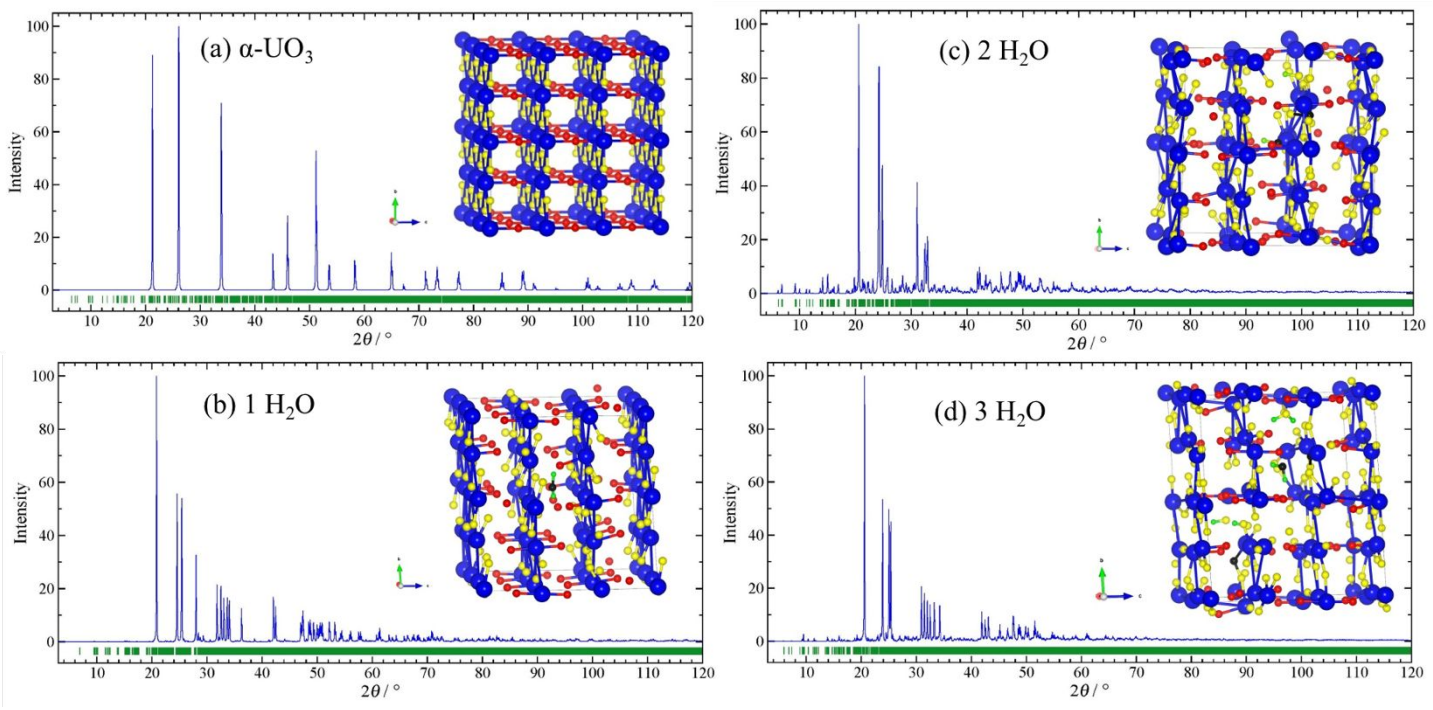


Figure 5. The relaxed structures and corresponding simulated XRD patterns calculated for $\alpha$-$UO_3$ before (a) and after addition of 1(b), 2(c), or 3(d) interstitial $H_2O$ molecules into the $\alpha$-$UO_3$ lattice. The U atoms are shown in blue, the O1 atoms are shown in red, the O2 atoms are shown in yellow, and the O atoms associated with $H_2O$ are shown in black. The hydrogen atoms associated with $H_2O$ are shown in green. For simplicity, only the initial bonds associated with the theoretical unperturbed $\alpha$-$UO_3$ structure are shown.

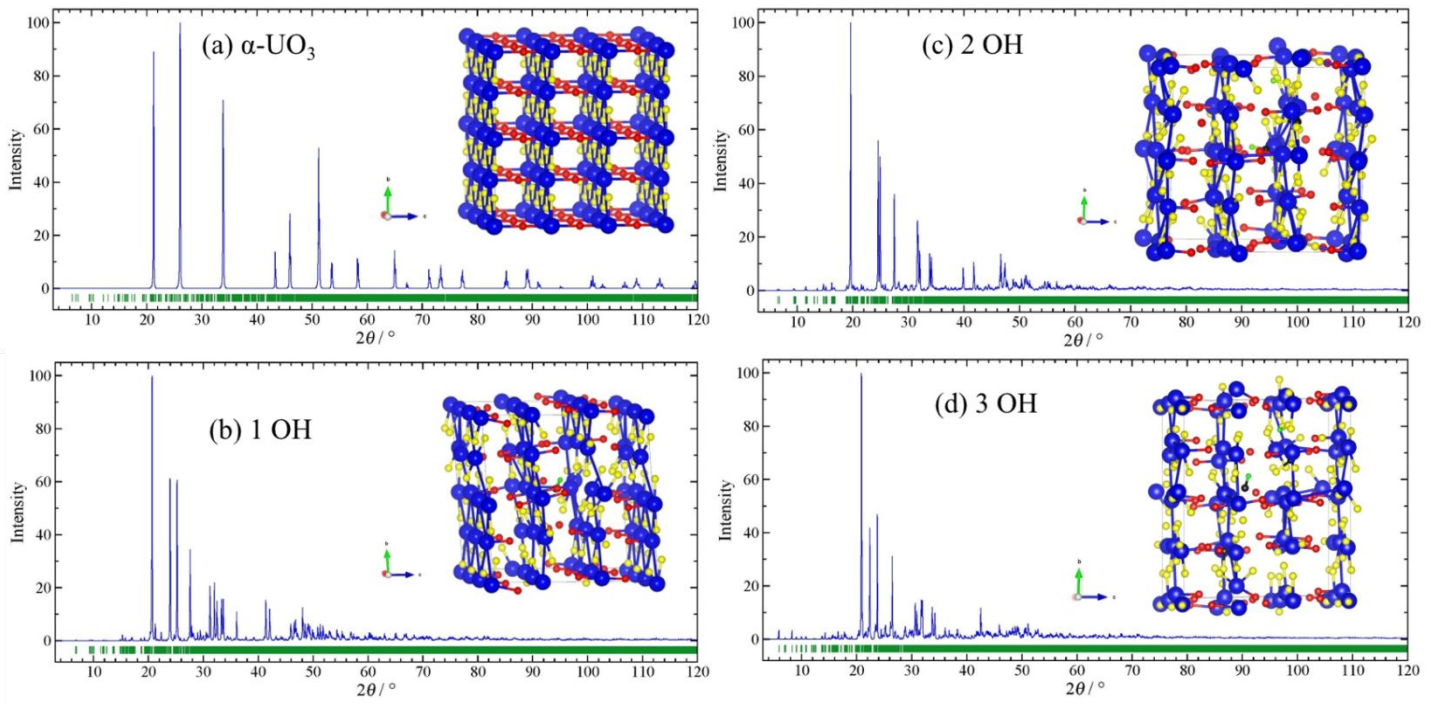


Figure 6. The relaxed structures and corresponding XRD patterns calculated for $\alpha$-$UO_3$ before (a) and after addition of 1

(b), 2 (c), or 3 (d) interstitial OH groups into the $\alpha$-$UO_3$ lattice. The U atoms are shown in blue, the O1 atoms are shown in red, the O2 atoms are shown in yellow, and the O atoms associated with OH are shown in black. The H atoms associated with OH are shown in green. For simplicity, only bonds that have not changed from the theoretical $\alpha$-$UO_3$ are shown.

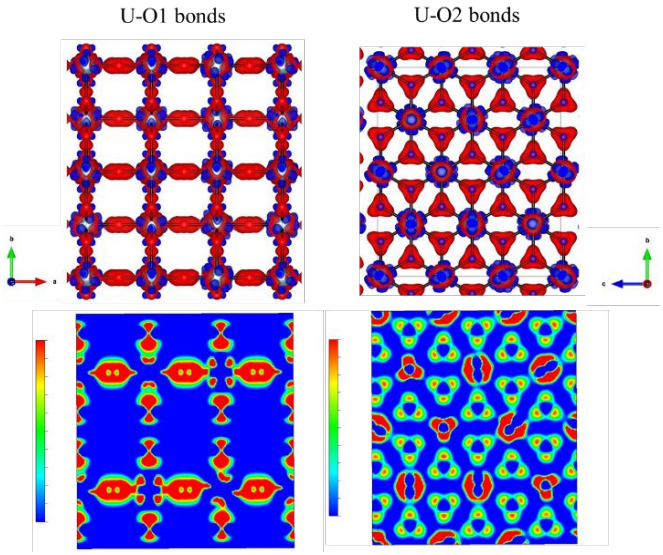


Figure 7. Three dimensional and two dimensional charge density difference plots of $\alpha$-$UO_3$ are shown for the U-O1 bonds (left) and the U-O2 bonds (right). The three dimensional images are shown on the top, and the two dimensional images are shown on the bottom. Regions of red indicate charge accumulation (positive) and regions of blue indicated charge depletion (negative). The iso-surface level is 0.135 $e^-/Å^3$.

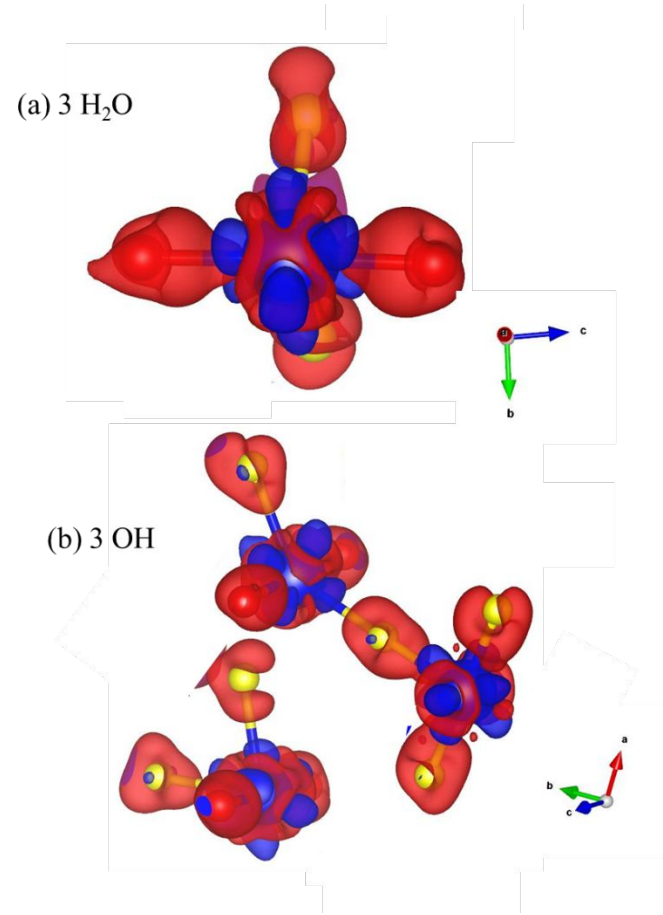


Figure 8. Three dimensional charge density difference plots of $\alpha$-$UO_3$ with (a) 3 $H_2O$ and (b) 3 OH are shown for the U-O1 (red atoms) bonds and the U-O2 (yellow atoms) bonds. Regions of red indicate charge accumulation (positive) and regions of blue indicate charge depletion (negative). The iso-surface level is 0.135 $e^-/Å^3$.

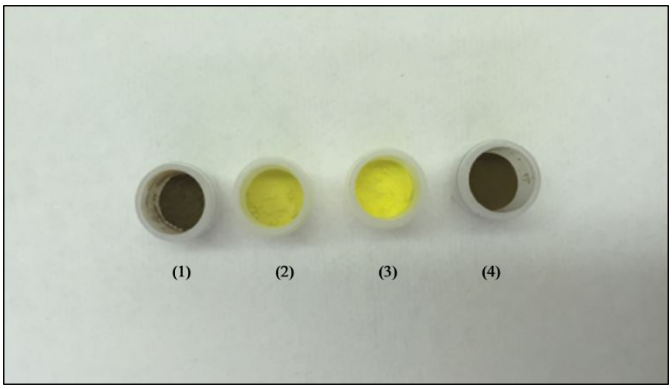


Graphic 1. Photograph of $\alpha$-$UO_3$ after storage under Conditions 1, 3 and 4 for over five years. (1) $\alpha$-$UO_3$ at time 0. (2) Condition 4 after five years. (3) Condition 3 after five years. (4) Condition 1 after five years.

## Conflicts of interest

There are no conflicts to declare.

## Acknowledgements

This work has been supported by the U.S. Department of Homeland Security, Domestic Nuclear Detection Office, under competitively awarded contracts IAA HSHQDC-13-00269 and HDHQDC-08-X-00805. S.C.H. would like to thank the Seaborg Institute at Los Alamos National Laboratory for providing funding to conduct the modelling studies. A.L.T. would like to thank the U.S. Department of Homeland Security under Grant Award Number 2012-DN-130-NF0001-02, the Seaborg Institute, and the University of Missouri for providing funding to perform this work. J.R.W.'s contribution to this material is based upon work supported by the U.S. Department of Homeland Security under Grant Award Number 2012-DN-130-NF-0001-02. The authors would like to thank Drs. Corwin Booth, David L. Clark, and Steven D. Conradson for useful discussions. All X-ray absorption data were collected at the Stanford Synchrotron Radiation Lightsource. Use of the Stanford Synchrotron Radiation Lightsource, SLAC National Accelerator Laboratory, is supported by the U.S. Department of Energy, Office of Science, Office of Basic Energy Sciences under Contract DE-AC02-76SF00515. The views and conclusions contained in this document are those of the authors and should not be interpreted as necessarily representing the official policies, either expressed or implied, of the U.S. Department of Homeland Security or the Government. Los Alamos National

Laboratory is operated by Triad National Security, LLC, for the National Nuclear Security Administration for the U.S. Department of Energy (Contract DE-SOL-001206). LA-UR-19-24180

## Notes and references

‡Note: In this report, schoepite is defined as $UO_3 \cdot xH_2O$, where $2 < x < 2.25$, while the term "schoepites" indicates the broad range of $UO_3$ hydrates.

## References


1 *Plutonium Handbook*, D. L. Clark, D. A. Geeson and R. J. Hanrahan, Jr., eds., American Nuclear Society, La Grange Park, Illinois USA, 2019.
2 I. Grenthe, J. Drożdżyński, T. Fujino, E. C. Buck, T. E. Albrecht-Schmitt and S. F. Wolf, Uranium, in *The Chemistry of the Actinide and Transactinide Elements*, L. R. Morss, N. M. Edelstein, J. Fuger and J. J. Katz, eds., Springer, Dordrecht, The Netherlands, 2006, 253-698.
3 D. L. Clark, S. S. Hecker, G. D. Jarvinen and M. P. Neu, Plutonium, in *The Chemistry of the Actinide and Transactinide Elements*, L. R. Morss, N. M. Edelstein, J. Fuger and J. J. Katz, eds., Springer, Dordrecht, The Netherlands, 2006, 813-1264.
4 N. S. Lloyd, J. F. W. Mosselmans, R. R. Parrish, S. R. N. Chenery, S. V. Hainsworth and S. J. Kemp, *Mineral. Mag.*, 2009, **73**, 495-510.
5 A. Leenaers, L. Sannen, S. Van den Berghe and M. Verwerft, *J. Nucl. Mater.*, 2003, **317**, 226-233.
6 R. J. McEachern and P. Taylor, *J. Nucl. Mater.*, 1998, **254**, 87-121.
7 D. J. Wronkiewicz, J. K. Bates, S. F. Wolf and E. C. Buck, *J. Nucl. Mater.*, 1996, **238**, 78-95.
8 P. Taylor, D. D. Wood and D. G. Owen, *J. Nucl. Mater.*, 1995, **223**, 316-320.
9 D. J. Wronkiewicz, J. K. Bates, T. J. Gernding, E. Veleckis and B. S. Tani, *J. Nucl. Mater.*, 1992, **190**, 107-127.
10 A. L. Tamasi, L. J. Cash, W. T. Mullen, A. L. Pugmire, A. R. Ross, C. E. Ruggiero, B. L. Scott, G. L. Wagner, J. R. Walensky and M. P. Wilkerson, *J. Radioanal. Nucl. Chem.*, 2017, **311**, 35-42.
11 A. L. Tamasi, K. S. Boland, K. Czerwinski, J. K. Ellis, S. A. Kozimor, R. L. Martin, A. L. Pugmire, D. Reilly, B. L. Scott, A. D. Sutton, G. L. Wagner, J. R. Walensky and M. P. Wilkerson, *Anal. Chem.*, 2015, **87**, 4210-4217.
12 K. Mayer, M. Wallenius and Z. Varga, *Chem. Rev.*, 2013, **113**, 884-900.
13 K. Mayer, *Nature,* 2013, **503**, 461-462.
14 Joint Working Group of the American Physical Society and the American Association for the Advancement of Science, *Nuclear Forensics: Role, State of the Art, Program Needs*, http://www.aaas.org/sites/default/files/migrate/uploads/Nuclear_Forensics.pdf.
15 W. Kugler, *Adv. X-ray Anal.*, 2003, **46**, 1-16.
16 N. A. Brincat, S. C. Parker, M. Molinari, G. A. Allen and M. T. Storr, *Inorg. Chem.*, 2014, **53**, 12253-12264.
17 C. Greaves and B. E. F. Fender, *Acta Cryst.*, 1972, **B28**, 3609-3614.
18 S. Siegel and H. R. Hoekstra, *Inorg. Nucl. Chem., Letters* 1971, **7**, 497-504.
19 H. R. Hoekstra, S. Siegel and F. X. Gallagher, *J. Inorg. Nucl. Chem.*, 1970, **32**, 3237-3248.
20 B. O. Loopstra and E. H. P. Cordfunke, *Recl. Trav. Chim. Pays-Bas*, 1966, **85**, 135-142.
21 V. J. Wheeler, R. M. Dell and E. Wait, *J. Inorg. Nucl. Chem.*, 1964, **26**, 1829-1845.
22 H. R. Hoekstra and S. Siegel, *J. Inorg. Nucl. Chem.*, 1961, **18**, 154-165.
23 P. Perio, *Bull. Soc. Chim. Fr.*, 1953, 776-777.
24 W. H. Zachariasen, *Acta Cryst.*, 1948, **1**, 265-268.
25 P. C. Debets, *Acta Cryst.*, 1966, **21**, 589-593.
26 P. C. Debets, *J. Inorg. Nucl. Chem.*, 1964, **26**, 1468-1470.
27 B. O. Loopstra; J. C. Taylor and A. B. Waugh, *J. Solid State Chem.*, 1977, **20**, 9-19.
28 S. Siegel and H. R. Hoekstra, *Inorg. Nucl. Chem. Lett.*, 1971, **7**, 455-459.
29 R. Engmann and P. M. de Wolff, *Acta Cryst.* 1963, **16**, 993-996.
30 M. T. Weller, P. G. Dickens and D. J. Penny, *Polyhedron*, 1988, **7**, 243-244.
31 E. Wait, *J. Inorg. Nucl. Chem.*, 1955, **1**, 309-312.
32 S. Siegel, H. Hoekstra and E. Sherry, *Acta Cryst.*, 1966, **20**, 292-295.
33 L. M. Kovba, L. M. Vidavskii and E. G. Lavut, *Zh. Strukt. Khim.*, 1963, **4**, 627-629.
34 D. E. Connolly, *Acta Cryst.*, 1959, **12**, 949-950.
35 R. J. Finch, M. A. Cooper and F. C. Hawthorne, *Canad. Mineral.*, 1996, **34**, 1071-1088.
36 M. T. Weller, M. E. Light and T. Gelbrich, *Acta. Crystallogr. B*, 2000, **56**, 577-583.
37 P. C. Debets and B. O. Loopstra, *J. Inorg. Nucl. Chem.*, 1963, **25**, 945-953.
38 H. R. Hoekstra and S. Siegel, *J. Inorg. Nucl. Chem.*, 1973, **35**, 761-779.
39 P. G. Allen, D. K. Shuh, J. J. Bucher, N. M. Edelstein, C. E. A. Palmer, R. J. Silva, S. N. Nguyen, L. N. Marquez and E. A. Hudson, *Radiochim. Acta*, 1995, **75**, 47-53.
40 J. C. Taylor, J. W. Kelly and B. Downer, *J. Solid State Chem.*, 1972, **5**, 291-299.
41 J. C. Taylor, *Acta. Crystallogr. B*, 1971, **27**, 1088-1091.
42 J. C. Taylor and H. J. Hurst, *Acta. Crystallogr. B*, 1971, **27**, 2018-2022.
43 D. Vier, *Thermal Stability of Certain Oxide Hydrates on $H_2O$*, U.S.A.E.C. Report, A-1277, 1944.
44 M. J. Bannister and J. C. Taylor, *Acta. Crystallogr. B*, 1970, **26**, 1775-1781.
45 J. C. Taylor and M. J. Bannister, *Acta. Crystallogr. B*, 1972, **28**, 2995-2999.
46 G. Bergström and G. Lundgren, *Acta Chem. Scand.*, 1956, **10**, 673-680.
47 S. Siegel, H. R. Hoekstra and E. Gebert, *Acta. Crystallogr. B*, 1972, **28**, 3469-3473.
48 E. H. P. Cordfunke and P. C. Debets, *J. Inorg. Nucl. Chem.*, 1964, **26**, 1671-1677.
49 R. B. Roof, Jr., D. T. Cromer and A. C. Larson, *Acta Cryst.*, 1964, **17**, 701-705.
50 J. K. Dawson, E. Wait, K. Alcock and D. R. Chilton, *J. Chem. Soc.*, **1956**, 3531-3340.
51 K.-A. Kubatko, K. Helean, A. Navrotsky and P. C. Burns, *Am. Mineral.*, 2006, **91**, 658-666.
52 A. G. Sowder, S. B. Clark and R. A. Fjeld, *Environ. Sci. Technol.*, 1999, **33**, 3552-3557.
53 R. J. Finch, F. C. Hawthorne and R. C. Ewing, *Canad. Mineral.*, 1998, **36**, 831-845.
54 R. J. Finch, M. L. Miller and R. C. Ewing, *Radiochim. Acta*, 1992, **58-59**, 433-444.
55 R. Thomas, M. Rivenet, E. Berrier, I. de Waele, M. Arab, D. Amaraggi, B. Morel and F. Abraham, *J. Nucl. Mater.*, 2017, **483**, 149-157.
56 L. E. Sweet, T. A. Blake, C. H. Henager, Jr., S. Hu, T. J. Johnson, D. E. Meier, S. M. Peper and J. M. Schwantes, *J. Radioanal. Nucl. Chem.*, 2013, **296**, 105-110.

57 O. V. Nipruk, A. V. Knyazev, G. N. Chernorukov and Yu. P. Pykhova, *Radiochemistry*, 2011, **53**, 146-148.
58 E. H. P. Cordfunke and A. A. van der Giessen, *J. Inorg. Nucl. Chem.*, 1963, **25**, 553-555.
59 G. L. Wagner, S. A. Kinkead, M. T. Paffett, K. D. Rector, B. L. Scott, A. L. Tamasi and M. P. Wilkerson, *J. Fluor. Chem.*, 2015, **178**, 107-114.
60 L. M. Anovitz, L. R. Riciputi, D. R. Cole, M. S. Gruszkeiwicz and J. M. Elam, *J. Non-cryst. Solids*, 2006, **352**, 5652-5662.
61 *ASTM Standard E104*, ASTM International, West Conshohocken, PA, 2012.
62 P. A. Lee, P. H. Citrin, P. Eisenberger, B. M. Kincaid, *Rev. Mod. Phys.*, 1981, **53**, 769–806.
63 G. G. Li, F. Bridges and C. H. Booth, *Phys. Rev. B*, 1995, **52**, 6332-6348.
64 T. M.; Hayes and J. B. Boyce, Extended X-ray absorption fine-structure spectroscopy, In *Solid State Physics*, H. Ehrenreich, F. Sietz and D. Turnbull, eds., Academic: New York, 1982, **37**, 173.
65 *RSXAP Analysis Package*, see http://lise.lbl.gov/RSXAP/(2012).
66 S. I. Zabinsky, J. J. Rehr, A. Ankudinov, R. C. Albers and M. J. Eller, *Phys. Rev. B*, 1995, **52**, 2995-3009.
67 P.-Y. Chevalier, E. Fischer and B. Cheynet, *J. Nucl. Mater.*, 2002, **303**, 1-28.
68 G. Kresse and J. Furthmuller, *Phys. Rev. B.*, 1996, **54**, 11,169-11,186.
69 G. Kresse and J. Furthmuller, *Comput. Mater. Sci.*, 1996, **6**, 15-50.
70 P. E. Blöchl, *Phys. Rev. B*, 1994, **50**, 17953-17,979.
71 G. Kresse and J. Hafner, *Phys. Rev. B*, 1994, **49**, 14,251-14,269.
72 G. Kresse and J. Hafner, *Phys. Rev. B*, 1993, **47**, 558-561.
73 J. P. Perdew, K. Burke and M. Ernzerhof, *Phys. Rev. Lett.*, 1996, **77**, 3865-3868.
74 S. L. Dudarev, G. A. Botton, S. Y. Savrasov, C. J. Humphreys and A. P. Sutton, *Phys. Rev. B*, 1998, **57**, 1505-1509.
75 K. Momma and F. Izumi, *J. Appl. Crystallogr.*, 2011, **44**, 1272-1276.
76 F. Izumi and K. Momma, *Solid State Phenom.*, 2007, **130**, 15-20.
77 Y.-J. Hu and C. H. Booth, *J. Phys. Conf.*, 2009, **190**, 1-4.

Experimental measurements and theoretical evaluation of changes in chemical speciation of $\alpha$-$UO_3$ using XRD, EXAFS, TGA, and DFT calculations